Mineralogical Magazine, December 2014, Vol. 78(7), pp. 1775–1793

Lead-antimony sulfosalts from Tuscany (Italy). XVI. Carducciite, $(AgSb)Pb_6(As,Sb)_8S_{20}$, a new Sb-rich derivative of rathite from the Pollone mine, Valdicastello Carducci: occurrence and crystal structure

Cristian Biagioni[1,*], Paolo Orlandi[1], Yves Moëlo[2] and Luca Bindi[3]

[1] Dipartimento di Scienze della Terra, Università di Pisa, Via S. Maria 53, I-56126 Pisa, Italy
[2] Institut des Matériaux Jean Rouxel, UMR 6502, CNRS, Université de Nantes, 2, rue de la Houssinière, 44 322 Nantes Cedex 3, France
[3] Dipartimento di Scienze della Terra, Università di Firenze, Via G. La Pira 4, I-50121 Florence, Italy

[*Received 21 January 2014; Accepted 25 June 2014; Associate Editor: A. Pring*]

ABSTRACT

The new mineral species carducciite, $(AgSb)Pb_6(As,Sb)_8S_{20}$, has been discovered in the baryte-pyrite-(Pb-Ag-Zn) deposit of the Pollone mine, near Valdicastello Carducci, Apuan Alps, Tuscany, Italy. It occurs as black metallic prismatic crystals, up to 0.5 mm long, associated with pyrite and sterryite. Its Vickers hardness (VHN_{10}) is 61 kg/mm^2 (range: 52−66), corresponding to a Mohs hardness of ~2½−3. In reflected light, carducciite is dark grey in colour, moderately bireflectant; internal reflections are very weak and deep red in colour. Reflectance percentages for the four COM wavelengths [R_{min}, R_{max} (%) (λ)] are: 35.8, 40.8 (471.1 nm), 33.7, 39.0 (548.3 nm), 32.7, 37.6 (586.6 nm) and 30.4, 35.1 (652.3 nm). Electron microprobe analysis gives (wt.% – mean of six analyses): Ag 3.55(12), Tl 0.13(3), Pb 41.90(42), Sb 17.79(19), As 12.41(14), S 22.10(17), total 97.9(6). On the basis of ΣMe = 16 a.p.f.u., the chemical formula is $Ag_{0.96}Tl_{0.02}Pb_{5.91}As_{4.84}Sb_{4.27}S_{20.14}$. The main diffraction lines, corresponding to multiple *hkl* indices, are (relative visual intensity): 3.689 (s), 3.416 (s), 3.125 (s), 2.989 (s), 2.894 (s), 2.753 (vs), 2.250 (s). The crystal-structure study gives a monoclinic unit cell, space group $P2_1/c$, with *a* 8.4909(3), *b* 8.0227(3), *c* 25.3957(9) Å, β 100.382(2)°, *V* 1701.63(11) Å^3, *Z* = 2. The crystal structure has been solved and refined to a final R_1 = 0.063 on the basis of 4137 observed reflections. It can be described within the framework of the sartorite homologous series, as formed by chemically twinned layers of the dufrénoysite type. The simplified idealized structural formula, based on 20 sulfur atoms, can ideally be written as $(AgSb)Pb_6(As,Sb)_{\Sigma=8}S_{20}$. Carducciite is an (Ag,Sb)-rich homeotype of dufrénoysite, stabilized by the complete coupled substitution 2 Pb^{2+} = Ag^+ + Sb^{3+} on a specific site of the crystal structure. Together with barikaite, it belongs to the rathite sub-group of $P2_1/c$ homeotypes of dufrénoysite, of which the crystal chemistry is discussed. The distribution of Ag, coupled with As or Sb on specific sites, appears to be the main criterion for the distinction between the three species of this sub-group.

Keywords: carducciite, new mineral, rathite, sulfosalt, lead, silver, antimony, arsenic, crystal structure, Pollone mine, Apuan Alps, Tuscany, Italy.

Introduction

During the last five years, a series of new or very rare Ag-Pb/Sb-As and Tl-Pb/Sb-As sulfosalts has been identified from the baryte-pyrite-iron oxide

* E-mail: biagioni@dst.unipi.it
DOI: 10.1180/minmag.2014.078.7.19

deposits of the southern Apuan Alps, Tuscany, Italy: sterryite, parasterryite and meerschautite from the Pollone mine, near Valdicastello Carducci (Moëlo *et al*., 2011; Biagioni *et al*., 2013*a*); and boscardinite and protochabournéite from the Monte Arsiccio mine (Orlandi *et al*., 2012, 2013).

During a routine check of mineral samples from the Pollone mine, some crystals were initially identified as an Sb-rich variety of rathite (Biagioni *et al*., 2012). Rathite is a very rare Ag-(Tl)-Pb sulfosalt first described by Baumhauer (1896) from Lengenbach, Binntal, Switzerland. Recently, rathite was also identified from the dolostone outcrop of Reckibach, Binntal, Switzerland (Cannon *et al*., 2008). Consequently, Pollone mine could be the third natural occurrence of this sulfosalt that is deserving of a more accurate characterization. In addition, preliminary chemical analysis showed an unusual richness in antimony, a surprising feature given that rathite from Lengenbach shows only minor Sb. Therefore, a crystallographic study has been undertaken, which shows the peculiar crystal-chemical role played by Sb.

Crystallographic study, chemical analysis and crystal-chemical considerations point to the distinction between rathite and this Sb-rich derivative, which has been named carducciite. The mineral and its name have been approved by the CNMNC-IMA, under the number 2013-006 (Biagioni *et al*., 2013*b*). The holotype specimen of carducciite is deposited in the mineralogical collection of the Museo di Storia Naturale, Università di Pisa, Via Roma 79, Calci, Pisa, Italy, under catalogue number 19646. The name is for the type locality, Valdicastello Carducci. This is the type locality of two other sulfosalts, parasterryite (Moëlo *et al*., 2011) and meerschautite (Biagioni *et al*., 2013*a*). The name also remembers the family name Carducci: the Italian poet Giosué Carducci (1835–1907), Nobel Prize winner for literature in 1906, was born at Valdicastello. His father, Michele (1808–1858), was employed as a doctor at the Pollone Pb-Ag mine from 1833 to 1836.

After the submission of the approval proposal of carducciite to the CNMNC-IMA, we became aware of the approval of barikaite (IMA 2012-055; Topa *et al*., 2013), a closely related but distinct phase, found in the Barika Au-Ag deposit, Azarbaijan Province, western Iran. In this paper we describe carducciite from the baryte-pyrite-(Pb-Zn-Ag) deposit of Pollone, Valdicastello Carducci, and discuss its crystal-chemical relationship with rathite and barikaite.

Geological setting

The baryte-pyrite-(Pb-Ag-Zn) deposit of Pollone (43º57’N; 10º16’E) is located in the southern portion of the Sant’Anna tectonic window, an area in which metamorphic rocks are surrounded by the non-metamorphic sedimentary formations of the Tuscan Nappe. The deposit is hosted in the Scisti di Fornovolasco Formation, belonging to the Fornovolasco-Panie Unit. This formation is related to the Variscan basement of the Apuan Unit (Pandeli *et al*., 2004) and consists of a Palaeozoic to Early Triassic(?) metavolcanic-metasedimentary sequence metamorphosed to greenschist facies. During the late stages of the Alpine orogeny, the development of shear zones led to the formation of numerous quartz + baryte veins; fluids were focused along these shear zones giving rise to syn-metamorphic and syn-tectonic veins. Estimates of $P-T$ conditions indicate that host and country rocks record metamorphic temperatures and pressures of ~350ºC and 0.35 GPa, respectively; appreciably higher temperatures (~450ºC) were found for the mineralizing fluids (Costagliola *et al*., 1998).

A great variety of sulfosalts have been described from all the baryte-pyrite-iron oxide deposits from the southern Apuan Alps (Table 1), and in particular from the Buca della Vena, Monte Arsiccio and Pollone mines. It is interesting to note that every deposit has some chemical peculiarities. Indeed, Buca della Vena mine is characterized by the occurrence of oxy-sulfosalts and oxy-chloro-sulfosalts; the Monte Arsiccio mine is particularly attractive for the occurrence of thallium sulfosalts, and the Pollone mine shows the presence of complex silver-lead sulfosalts. Carducciite is one of these rare mineral species.

Occurrence and mineral description

Physical and optical properties

Carducciite has been identified in only a few specimens from the Pizzone stope, in an area rich in acicular sulfosalts. It was observed embedded in saccharoidal baryte or rarely in small vugs, as black prismatic crystals, striated parallel to the elongation, up to 0.5 mm long and 0.2 mm wide (Fig. 1). It is brittle, with a conchoidal fracture. The streak is black and the lustre is metallic.

Micro-indentation measurements carried out with a VHN load of 10 g give a mean value of 61 kg/mm^2 (range: 52–66) corresponding to a Mohs hardness of ~2½–3.

TABLE 1. Lead sulfosalts from baryte-pyrite-iron oxide deposits from the southern Apuan Alps. Abbreviations for localities: BdV = Buca della Vena mine; Fv = Fornovolasco mine; MA = Monte Arsiccio mine; Pl = Pollone mine.

	Chemical formula	Localities
Lead sulfosalts		
Boulangerite	$Pb_5Sb_4S_{11}$	BdV, Fv, MA, Pl
Geocronite	$Pb_{14}Sb_6S_{23}$	Pl
Jordanite	$Pb_{14}As_6S_{23}$	Pl
Robinsonite	$Pb_4Sb_6S_{13}$	BdV, MA
Twinnite	$Pb(Sb_{0.63}As_{0.37})_2S_4$	MA, Pl
Zinkenite	$Pb_9Sb_{22}S_{42}$	BdV, MA, Pl
Lead-copper sulfosalts		
Bournonite	$CuPbSbS_3$	BdV, Fv, Pl
Jaskólskíite	$Cu_xPb_{2+x}(Sb,Bi)_{2-x}S_6$	Fv
Meneghinite	$CuPb_{13}Sb_7S_{24}$	Fv, Pl
Tintinaite	$Cu_2Pb_{10}Sb_{16}S_{35}$	BdV
Lead-iron sulfosalts		
Jamesonite	$FePb_4Sb_6S_{14}$	Fv
Lead-mercury and lead-copper-mercury sulfosalts		
Marrucciite†	$Hg_3Pb_{16}Sb_{18}S_{46}$	BdV
Rouxelite†	$Cu_2HgPb_{23}Sb_{27}S_{65.5}$	BdV, MA
Lead-silver sulfosalts		
Carducciite*†	$(AgSb)Pb_6(As,Sb)_8S_{20}$	Pl
Diaphorite	$Ag_3Pb_2Sb_3S_8$	Pl
Meerschautite*†	$(Ag,Cu)_6Pb_{43-2x}Sb_{44+2x}S_{112}O_x$ ($x \sim 0.5$)	Pl
Owyheeite	$Ag_3Pb_{10}Sb_{11}S_{28}$	Pl
Parasterryite*†	$Ag_4Pb_{20}(Sb,As)_{24}S_{58}$	Pl
Sterryite*	$Cu(Ag,Cu)_3Pb_{19}(Sb,As)_{22}(As\text{-}As)S_{56}$	Pl
Lead-thallium sulfosalts		
Boscardinite*†	$TlPb_4(Sb_7As_2)_{\Sigma 9}S_{18}$	MA
Protochabournéite*†	$Tl_2Pb(Sb_{9\text{-}8}As_{1\text{-}2})_{\Sigma 10}S_{17}$	MA
Lead oxysulfosalts, chlorosulfosalts and oxy-chlorosulfosalts		
Dadsonite	$Pb_{23}Sb_{25}S_{60}Cl$	BdV
Pellouxite†	$(Cu,Ag)_2Pb_{21}Sb_{23}S_{55}ClO$	BdV
Pillaite†	$Pb_9Sb_{10}S_{23}ClO_{0.5}$	BdV
Scainiite†	$Pb_{14}Sb_{30}S_{54}O_5$	BdV

Notes: chemical formulae are from Moëlo *et al*. (2008), with the exception of sulfosalt species denoted with *, where the chemical formulae are after Moëlo *et al*. (2012) [parasterryite and sterryite], Orlandi *et al*. (2012) [boscardinite], Orlandi *et al*. (2013) [protochabournéite], Biagioni *et al*. (2013*a*) [meerschautite] and this work [carducciite]. The symbol † indicates sulfosalts described for the first time from the baryte-pyrite-iron oxides of Apuan Alps.

In plane-polarized incident light, carducciite is dark grey in colour, moderately bireflectant and pleochroic from light grey to a slightly greenish grey. Between crossed polars, carducciite is anisotropic with greyish to light-blue rotation tints. Internal reflections are very weak and deep red in colour. There is no optical evidence of growth zonation.

Reflectance measurements were performed in air by means of a MPM-200 Zeiss microphotometer equipped with a MSP-20 system processor on a Zeiss Axioplan ore microscope. The filament temperature was ~3350 K. An interference filter was adjusted, in turn, to select four COM (IMA Commission on Ore Microscopy) wavelengths for measurement (471.1, 548.3, 586.6 and 652.3 nm).

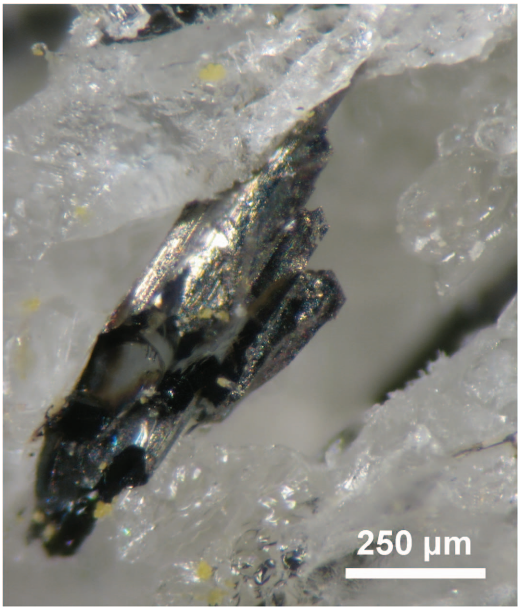

FIG. 1. Carducciite, black prismatic crystals up to 0.5 mm. The conchoidal fracture of carducciite is clearly visible.

Readings were taken for specimen and standard (SiC) maintained under the same focus conditions. The diameter of the circular measuring area was 0.1 mm. Reflectance percentages for $R_{\min}$ and $R_{\max}$ (%) are 35.8, 40.8 (471.1 nm), 33.7, 39.0 (548.3 nm), 32.7, 37.6 (586.6 nm) and 30.4, 35.1 (652.3 nm), respectively.

Owing to its softness and fragility, only minute grains could be extracted from baryte for X-ray study and preparation as polished sections for microprobe analysis and reflectance measurement. These grains were unsuitable for measuring the density. Calculated density (based on the empirical formula) is 5.56 g/cm^3.

Carducciite is associated with baryte, pyrite, sphalerite, sterryite and twinnite. Up to now, only a few sub-millimeter-sized fragments of carducciite have been identified; it is probably the rarest sulfosalt found so far at the Pollone mine.

Chemical analysis

A crystal of carducciite was analysed with a CAMEBAX SX50 electron microprobe (BRGM-CNRS-University common laboratory, Orléans, France). The operating conditions were: accelerating voltage 20 kV, beam current 20 nA, beam size 5 µm. Standards (element, emission line, counting times for one spot analysis) are: pyrite (S$K\alpha$, 20 s), stibnite (Sb$L\alpha$, 20 s), AsGa (As$L\alpha$, 30 s), Ag metal (Ag$L\alpha$, 20 s), galena (Pb$M\alpha$, 20 s) and lorándite (Tl$M\alpha$, 20 s).

Electron microprobe data for carducciite are given in Table 2. Notwithstanding the low total, probably due to the poor quality of the polished surface, the results are in agreement with the structural analysis (see below). On the basis of ΣMe = 16 atoms per formula unit (a.p.f.u.), the chemical formula can be written as $Ag_{0.96(3)}Tl_{0.02(1)}Pb_{5.91(4)}(As_{4.84(4)}Sb_{4.27(5)})_{\Sigma=9.11}S_{20.14(15)}$. If Tl and Ag are subtracted according to the substitution rule (Tl, Ag)$^+$ + (As, Sb)$^{3+}$ = 2 Pb^{2+}, the chemical formula can be written $Pb_{7.87}(As,Sb)_{\Sigma=8.13}S_{20.14(14)}$, agreeing with the general formula of the N = 4 dufrénoysite homologue of the sartorite series (Makovicky, 1985), $Pb_8As_8S_{20}$.

Crystallography

The powder X-ray diffraction pattern of carducciite was obtained using a 114.6 mm diameter Gandolfi camera, with Ni-filtered Cu$K\alpha$ radiation. The observed powder X-ray diffraction pattern is compared with the calculated one (obtained using the software *PowderCell*; Kraus and Nolze, 1996) in Table 3. Unit-cell parameters were not refined from the powder X-ray diffraction data because of the multiplicity of indices for the majority of the diffraction lines.

For the single-crystal X-ray diffraction study, the intensity data were collected using a Bruker Smart Breeze diffractometer equipped with an air-cooled CCD detector, with Mo$K\alpha$ radiation. The detector to crystal distance was 50 mm. 878 frames were collected using ω scan mode, in 0.5º slices, with an exposure time of 10 s per frame. The data were corrected for Lorentz and polarization factors and absorption using the software package *Apex2* (Bruker AXS Inc., 2004). The statistical tests on the distribution of $|E|$ values ($|E^2-1|$ = 0.868) and the systematic absences suggested the space group $P2_1/n$, which was subsequently transformed by the matrix $\mathbf{R}$ = $(1\ 0\ 0,\ 0\ \bar{1}\ 0,\ \bar{1}\ 0\ \bar{1})$ into the standard setting $P2_1/c$. The refined cell parameters, in the standard setting, are a 8.4909(3), b 8.0227(3), c 25.3957(9) Å, β 100.382(2)º, V 1701.63(11) Å^3.

The crystal structure was refined using *SHELXL-97* (Sheldrick, 2008) starting from the atomic coordinates given by Berlepsch *et al.*

TABLE 2. Microprobe analysis of carducciite: chemical composition as wt.% and chemical formula (in atoms per formula unit, a.p.f.u.) on the basis of $\Sigma Me = 16$ a.p.f.u.

Element	Range	Mean (n = 6)	e.s.d.
Ag	3.33–3.66	3.55	0.12
Tl	0.11–0.18	0.13	0.03
Pb	41.55–42.62	41.90	0.42
Sb	17.56–18.13	17.79	0.19
As	12.27–12.59	12.41	0.14
S	21.96–22.37	22.10	0.17
Total	97.53–99.08	97.87	0.61
Ag	0.905–0.990	0.961	0.031
Tl	0.015–0.025	0.018	0.004
Pb	5.975–5.870	5.910	0.041
Sb	4.225–4.360	4.270	0.052
As	4.795–4.890	4.841	0.035
S	19.940–20.410	20.143	0.147
Ev*	−1.4–0.1	−0.4	0.7
$Pb_{corr.}$**	5.900–6.015	5.947	0.043
$(Sb + As)_{corr.}$**	9.070–9.140	9.093	0.025
$Sb/(Sb + As)_{at.}$	0.464–0.476	0.469	0.005

* Relative error on the valence equilibrium (%), calculated as $[\Sigma(\text{val}+) - \Sigma(\text{val}-)] \times 100 / \Sigma(\text{val}-)$.
** $Pb_{corr.}$ and $(Sb+As)_{corr.}$ on the basis of the substitution $Tl^{+} + (As,Sb)^{3+} = 2\ Pb^{2+}$.

(2002). Scattering curves for neutral atoms were taken from the *International Tables for Crystallography* (Wilson, 1992). Crystal data and details of the intensity data collection and refinement are reported in Table 4. After several cycles of isotropic refinement, the R_1 converged to 0.14; by refining the anisotropic displacement parameters for the metals only, the refinement yielded an R_1 value of 0.074, thus confirming the correctness of the structural model. Successive cycles of refinement converged to R_1 = 0.071, with an anisotropic model for all the atoms. The M5 site was found to split in two positions (i.e. M5a and M5b). The refinement of the occupancy factors at these sites (using Sb *vs.* structural vacancy) led to 24.7 and 24.2 electrons, respectively. Examination of bond distances suggests that M5a is occupied by the larger cation Ag, whereas M5b is occupied by Sb. The successive refinement cycles were carried out using Ag *vs.* vacancy (M5a) and Sb *vs.* vacancy (M5b) which lowers the R_1 to 0.069, and gave an overall composition for the M5 site of $Ag_{0.53}Sb_{0.47}$, in good agreement with the expected value. Finally, the occupancies were refined for M2, M3, M4 (As *vs.* Sb) and M6 (Pb *vs.* As).

According to Marumo and Nowacki (1965), rathite ("rathite–I" of these authors), homeotypic with carducciite (see below), is usually polysynthetically twinned. To verify such pseudo-merohedral twinning, the twin law ($\bar{1}$ 0 0, 0 $\bar{1}$ 0, 1 0 1) was added in the refinement but no improvement was found, thus indicating that the crystal studied is actually untwinned. Notwithstanding the observation of Marumo and Nowacki (1965), Berlepsch *et al.* (2002), through single-crystal X-ray diffraction data, Pring (2001), through high-resolution transmission electron microscopy and Topa *et al.* (2013), through reflected light microscopy, observed no twinning in rathite and barikaite, respectively.

The refinement finally converged to R_1 = 0.063 for 4137 reflections with $F_o > 4\sigma(F_o)$ and 0.103 for all 6078 independent reflections. The highest and deepest residuals are located around the Pb2 site. Atomic coordinates and bond distances are reported in Table 5 and Table 6, respectively, and the unit-cell content with atom labels is given in Fig. 2. Bond-valence sums are given in Table 7.

The crystal-chemical formula of carducciite, as obtained through this refinement of the crystal

TABLE 3. Powder X-ray diffraction data for carducciite.

I_{obs}	d_{meas}	I_{calc}	d_{calc}	*h k l*
		6	12.49	0 0 2
mw	7.6	17	7.64	0 1 1
mw	6.8	16	6.75	0 1 2
mw	5.79	15	5.78	0 1 3
w	5.42	9	5.50	$\bar{1}$ 0 4
mw	4.92	19	4.93	0 1 4
m	4.21	21	4.24	0 1 5
		38	4.19	$\bar{2}$ 0 2
		17	4.18	2 0 0
m	4.01	17	4.03	$\bar{1}$ 0 6
		23	4.01	0 2 0
		8	3.961	0 2 1
ms	3.815	78	3.819	0 2 2
		6	3.802	$\bar{2}$ 0 4
s	**3.689**	100	3.695	0 1 6
ms	3.592	11	3.619	$\bar{1}$ 2 1
		20	3.614	0 2 3
		30	3.605	$\bar{2}$ 1 3
		36	3.582	2 1 1
s	**3.416**	70	3.436	$\bar{2}$ 1 4
		69	3.406	2 1 2
		8	3.375	0 2 4
vw	3.241	5	3.256	$\bar{2}$ 0 6
m	3.221	25	3.233	$\bar{2}$ 1 5
		23	3.200	2 1 3
s	**3.125**	67	3.128	0 2 5
		45	3.122	0 0 8
s	**2.989**	60	3.017	$\bar{2}$ 1 6
		93	2.984	2 1 4
s	**2.894**	21	2.916	$\bar{2}$ 2 1
		29	2.910	$\bar{1}$ 1 8
		13	2.899	$\bar{2}$ 2 2
		9	2.893	2 2 0
		62	2.889	0 2 6
mw	2.833	13	2.845	$\bar{2}$ 2 3
		15	2.834	2 2 1
w	2.798	17	2.804	$\bar{2}$ 1 7
vs	**2.753**	20	2.771	2 1 5
		99	2.760	$\bar{2}$ 2 4
		85	2.744	2 2 2
ms	2.657	15	2.666	0 2 7
		7	2.663	$\bar{3}$ 1 1
		12	2.659	0 3 1
		16	2.651	$\bar{2}$ 2 5
mw	2.632	8	2.633	2 2 3
		9	2.630	3 1 0
		14	2.615	0 3 2
vw	2.462	6	2.458	0 3 4
vw	2.388	9	2.385	0 1 10
m	2.337	50	2.337	$\bar{2}$ 0 10
m	2.311	7	2.314	1 3 4
		43	2.309	2 0 8
		9	2.282	0 2 9
s	**2.250**	25	2.254	$\bar{2}$ 3 2
		22	2.252	2 3 0
		21	2.250	0 3 6
		11	2.244	$\bar{2}$ 1 10
vw	2.220	10	2.219	2 1 8
vw	2.182	5	2.185	0 1 11
w	2.12	65	2.122	$\bar{4}$ 0 2
		8	2.120	0 2 10
w	2.067	8	2.068	2 1 9
w	2.032	18	2.031	0 3 8
		6	2.019	$\bar{2}$ 2 10
w	1.983	11	1.980	0 4 2
		7	1.957	$\bar{4}$ 1 6
vw	1.951	9	1.950	0 4 3
vw	1.925	13	1.926	0 3 9
mw	1.912	13	1.917	$\bar{2}$ 3 8
		16	1.905	2 3 6
vw	1.883	5	1.880	$\bar{3}$ 3 5
		6	1.858	$\bar{4}$ 2 4
		10	1.852	4 2 0
w	1.846	12	1.850	$\bar{4}$ 1 8
		9	1.848	0 2 12
mw	1.833	7	1.838	$\bar{2}$ 3 9
		8	1.831	4 1 4
		7	1.829	$\bar{2}$ 1 13
		9	1.826	2 3 7
w	1.810	10	1.811	2 1 11
		7	1.809	$\bar{2}$ 4 2
m	1.796	10	1.808	2 4 0
		14	1.800	$\bar{2}$ 2 12
		8	1.796	$\bar{2}$ 4 3
		12	1.793	2 4 1
		17	1.784	2 2 10
		6	1.763	$\bar{4}$ 2 7
m	1.744	9	1.749	4 2 3
		6	1.746	$\bar{3}$ 2 11
		10	1.745	4 0 6
		16	1.742	0 1 14
mw	1.706	9	1.703	4 2 4
mw	1.661	7	1.659	2 4 5
w	1.575	7	1.564	0 4 10
mw	1.557	17	1.554	0 5 4
		5	1.550	$\bar{4}$ 3 8
		5	1.503	0 4 11

Notes: the d_{hkl} values were calculated on the basis of the unit cell refined by using single-crystal data. Intensities were calculated on the basis of the structural model. Observed intensities were estimated visually. vs = very strong; s = strong; ms = medium-strong; m = medium; mw = medium-weak; w = weak; vw = very weak. Only reflections with I_{calc} > 5 are listed, if not observed. The seven strongest reflections are shown in bold.

TABLE 4. Crystal data and summary of parameters describing data collection and refinement for carducciite.

Crystal data	
X-ray formula	$Ag_{1.05}Pb_{5.84}As_{4.63}Sb_{4.48}S_{20}$
Crystal size (mm)	$0.27 \times 0.16 \times 0.16$
Cell setting, space group	Monoclinic, $P2_1/c$
a, b, c (Å);	8.4909(3), 8.0227(3), 25.3957(9);
α, β, γ (º)	90.00, 100.382(2), 90.00
V (Å^3)	1701.63(11)
Z, Dc (g/cm^3)	2, 5.576
Data collection and refinement	
Radiation, wavelength (Å)	Mo$K\alpha$, λ = 0.71073
Temperature (K)	293
Maximum observed 2θ (º)	65.14
Measured reflections	17,409
Unique reflections	6078
Reflections $F_o > 4\sigma(F_o)$	4137
R_{int} after absorption correction	0.0533
$R\sigma$	0.0691
Range of h, k, l	$-12 \leqslant h \leqslant 12$, $-12 \leqslant k \leqslant 10$, $-33 \leqslant l \leqslant 38$
R [F_o>4 σ F_o]	0.0630
R (all data)	0.1026
wR (on F_o^2)	0.1460
Gof	1.107
Number of least-squares parameters	174
Maximum and minum residual peak (e/Å^3)	6.10 (at 0.74 Å from Pb2) −6.96 (at 0.77 Å from Pb2)

TABLE 5. Atomic positions and equivalent displacement parameters for carducciite.

Site	Occupancy	x/a	y/b	z/c	U_{eq} (Å^2)
Pb1	$Pb_{1.00}$	0.47837(7)	0.73364(7)	0.20441(2)	0.0330(2)
Pb2	$Pb_{1.00}$	0.97620(8)	0.73021(10)	0.20198(3)	0.0503(2)
M1	$As_{0.98(1)}Sb_{0.02(1)}$	0.29523(14)	0.83027(17)	0.34013(5)	0.0198(4)
M2	$As_{0.60(1)}Sb_{0.40(1)}$	0.24213(17)	0.31010(15)	0.14809(5)	0.0303(4)
M3	$Sb_{1.00}$	0.67428(11)	0.63675(12)	0.04195(4)	0.0288(2)
M4	$As_{0.66(1)}Sb_{0.34(1)}$	0.13884(14)	0.65000(17)	0.05807(6)	0.0314(4)
M5a	$Ag_{0.526(4)}$	0.4176(5)	0.0193(6)	0.0746(2)	0.0332(5)
M5b	$Sb_{0.474(4)}$	0.4164(5)	0.0316(6)	0.0541(2)	0.0332(5)
M6a	$Pb_{0.920(5)}$	0.90744(8)	0.07271(12)	0.07400(3)	0.0302(3)
M6b	$As_{0.080(5)}$	0.898(3)	0.013(4)	0.085(1)	0.0302(3)
S1	$S_{1.00}$	0.2596(4)	0.9911(4)	0.2658(1)	0.0227(6)
S2	$S_{1.00}$	0.2509(4)	0.4623(4)	0.2257(1)	0.0207(5)
S3	$S_{1.00}$	0.5000(4)	0.6612(4)	0.3214(1)	0.0223(6)
S4	$S_{1.00}$	0.9128(4)	0.1581(4)	0.1830(1)	0.0217(6)
S5	$S_{1.00}$	0.6880(4)	0.8348(4)	0.1153(1)	0.0230(6)
S6	$S_{1.00}$	0.1733(4)	0.8692(4)	0.1191(1)	0.0247(6)
S7	$S_{1.00}$	0.3756(4)	0.5061(4)	0.1013(1)	0.0226(6)
S8	$S_{1.00}$	0.9587(4)	0.4983(4)	0.0977(1)	0.0248(7)
S9	$S_{1.00}$	0.5942(4)	0.2000(5)	0.0098(2)	0.0306(8)
S10	$S_{1.00}$	0.1652(4)	0.1876(5)	0.0075(1)	0.0267(7)

TABLE 6. Selected bond distances (Å) in carducciite.

Pb1	– S1	2.950(3)	Pb2	– S4	2.960(3)	M1	– S4	2.236(4)	M2	– S2	2.309(3)
	– S3	2.999(3)		– S1	2.992(3)		– S1	2.262(4)		– S7	2.378(3)
	– S2	3.023(3)		– S5	3.098(3)		– S3	2.321(3)		– S3	2.492(3)
	– S7	3.183(4)		– S6	3.120(3)		– S8	3.191(4)		– S8	2.933(4)
	– S2	3.214(3)		– S2	3.149(3)		– S7	3.243(4)		– S4	3.315(3)
	– S5	3.226(3)		– S8	3.218(4)					– S6	3.639(4)
	– S6	3.250(3)		– S1	3.375(3)					– S10	3.646(4)
	– S1	3.344(3)		– S2	3.440(3)						
	– S3	3.503(3)		– S4	3.494(3)						
M3	– S5	2.435(3)	M4	– S8	2.321(4)	M5a	– S9	2.759(6)	M5b	– S9	2.446(6)
	– S7	2.458(3)		– S6	2.328(4)		– S5	2.770(5)		– S9	2.458(6)
	– S3	2.749(4)		– S7	2.405(4)		– S6	2.808(5)		– S10	2.571(6)
	– S8	2.799(3)		– S10	3.096(4)		– S9	2.819(6)		– S5	2.988(6)
	– S4	3.343(3)		– S9	3.310(4)		– S10	2.829(6)		– S6	3.149(5)
	– S6	3.634(4)					– S3	2.848(5)		– S3	3.283(5)
	– S10	3.764(4)									
M6a	– S4	2.844(3)	M6b	– S5	2.51(4)						
	– S6	2.854(3)		– S6	2.61(3)						
	– S10	2.927(4)		– S4	2.72(3)						
	– S5	2.986(3)		– S10	2.82(3)						
	– S9	3.036(4)		– S9	3.28(3)						
	– S10	3.134(3)		– S10	3.55(3)						
	– S8	3.481(4)									

structure, is $Ag_{1.05}Pb_{5.84}As_{4.63}Sb_{4.48}S_{20}$, with the relative error on the valence equilibrium Ev = +0.15. This formula is not exactly charge balanced, but it does not take into account the limited Pb for Tl substitution; the site(s) involved in this substitution has (have) not been localized, due to the very similar scattering factors of these two elements. In addition, it shows a slightly greater $Sb/(Sb+As)_{at.}$ ratio with respect to the results of chemical analysis, i.e. 0.49 *vs.* 0.47.

Crystal-structure description

General organization of carducciite

The general organization of the crystal structure of carducciite is presented in Fig. 3. It belongs to the N = 4 homologue of the sartorite series and it shows a homeotypic relationship with dufrénoysite (Moëlo *et al.*, 2008; Table 8). It can be described as formed by chemically twinned layers of the dufrénoysite type.

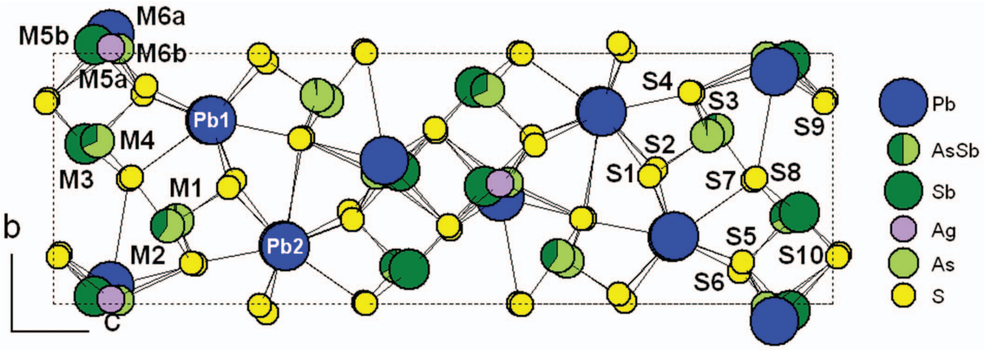

FIG. 2. Crystal structure of carducciite: projection of the unit cell along **a**. Note: for clarity, M5a, M5b, M6a and M6b have been represented as full circles, despite their partial filling.

TABLE 7. Bond-valence calculations according to Brese and O'Keeffe (1991).

	Pb1	Pb2	M1	M2	M3	M4	M5a	M5b	M6a	M6b	Σ_{anions}
S1	0.34 0.12	0.30 0.11	1.01								1.88
S2	0.28 0.17	0.20 0.09		1.11							1.85
S3	0.30 0.08		0.86	0.68			0.08	0.05			2.03
S4		0.33 0.08	1.08	0.07					0.42	0.04	2.02
S5	0.16	0.23			1.04		0.10	0.11	0.28	0.06	1.98
S6	0.15	0.21				1.02	0.09	0.07	0.40	0.05	1.99
S7	0.18		0.07	0.92	0.09	0.83					2.09
S8		0.16	0.08	0.21	0.39	1.04			0.07		1.95
S9					0.45	0.07	0.10 0.09	0.47 0.46	0.25	0.01	1.90
S10					0.98	0.13	0.08	0.34	0.33 0.19	0.03	2.08
Σ_{cations}	1.78	1.71	3.10	2.99	2.95	3.09	0.54	1.50	1.94	0.19	
Theor.*	2.00	2.00	3.00	3.00	3.00	3.00	0.53	1.41	1.84	0.24	

In mixed sites, the bond-valence contribution of each cation has been considered according to its occupancy (see Table 5).
* Theoretical valence on the basis of site occupancies.

The crystal structure of rathite (as well as that of barikaite) displays walls of 'standing' tricapped trigonal coordination prisms of Pb (prism axis parallel to **a**), alternating with slabs (dufrénoysite layers) composed of 'lying' trigonal coordination prisms of (As,Sb) and Pb, based on SnS archetype (Berlepsch *et al.*, 2002). The structure of carducciite is basically similar to that described by Marumo and Nowacki (1965) and Berlepsch *et al.* (2002) for rathite from Lengenbach and by

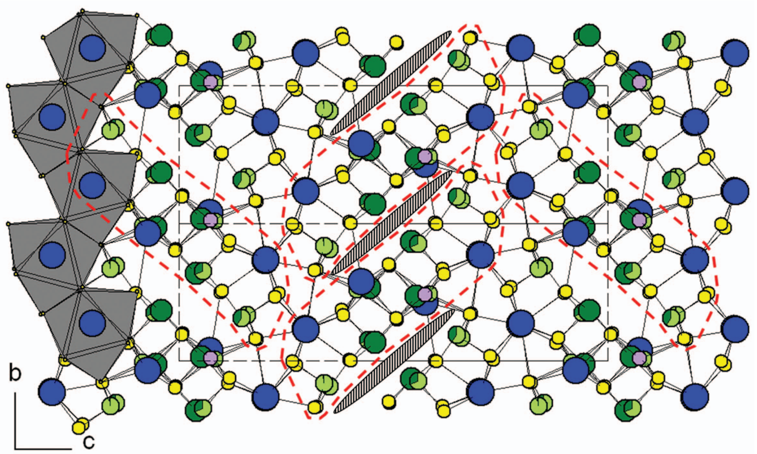

FIG. 3. Carducciite structure: general organization. Dashed red lines delimit the N = 4 dufrénoysite-type ribbons, separated along **b** by lone-electron-pair micelles (black hatched ellipses). Left: connection along **b** of Pb tricapped triangular prisms (grey).

TABLE 8. Cell parameters of N = 4 sartorite homologues ($P2_1/c$ setting for rathite isotypes).

Mineral	Chemical formula	*a* (Å)	*b* (Å)	*c* (Å)	β (º)	S.G.	Ref.
Dufrénoysite	$Pb_8As_8S_{20}$	7.90	25.74	8.37	90.35	$P2_1$	(1)
Veenite	$Pb_8(Sb,As)_8S_{20}$	8.44	26.2	7.90	unknown	unknown	(2)
Rathite	$(AgAs)Pb_6As_8S_{20}$	8.50	7.97	25.12	100.70	$P2_1/c$	(3)
Barikaite	$Ag_{1.5}Pb_5As_{5.5}Sb_4S_{20}$	8.53	8.08	24.95	100.66	$P2_1/c$	(4)
Carducciite	$(AgSb)Pb_6As_8S_{20}$	8.49	8.02	25.40	100.38	$P2_1/c$	(5)

(1) Marumo and Nowacki (1967); (2) Jambor (1967); (3) Berlepsch *et al.* (2002); (4) Topa *et al.* (2013); (5) this work.

Makovicky and Topa (2013) for barikaite. The walls of 'standing' tricapped trigonal prisms, centred by Pb atoms (and possibly minor Tl) are formed by columns composed of the alternation, along **a**, of Pb1 and Pb2 polyhedra sharing faces. Adjacent columns are connected along **b** through edge-sharing, giving rise to the walls. Between the walls, dufrénoysite layers (N = 4) occur.

The dufrénoysite layer type occurs in different sulfosalts belonging to the sartorite homologous series: dufrénoysite, rathite, barikaite, liveingite, baumhauerite, baumhauerite-2*a* and boscardinite. In carducciite, within the dufrénoysite layer, there are two pure (or nearly pure) As (M1) and Sb (M3) sites, two mixed (As,Sb) sites (M2 and M4, with As > Sb), and two split sites, i.e. an Ag/Sb split site (M5) and a Pb/As one with Pb > As (M6). Such an equivalent (Ag,Sb) and (Pb,As) pair is in the same configuration of the constitutive layer of rathite, barikaite (in both phases, however, the split site M5 is occupied by Ag and As) and, in particular, of boscardinite (Orlandi *et al.*, 2012).

Cation coordination and site occupancies

The crystal structure of carducciite contains two pure Pb sites, four Me^{3+} sites [where *Me* is As, Sb, or (As, Sb)], two split sites (an Ag/Sb and a Pb/As site) and 10 S sites (Table 5). Pb1 and Pb2 are 'standing' tricapped trigonal coordination prisms, with average bond lengths of 3.188 and 3.205 Å, respectively. The four sites hosting As and/or Sb can be divided into two mixed (As, Sb) sites, a nearly pure As site and a pure Sb site.

The M1 site, with a mean bond length of 2.27 Å (in good agreement with rathite of Berlepsch *et al.*, 2002 and barikaite, i.e. 2.26 and 2.28 Å, respectively) and a three-fold coordination, is a nearly pure As site; the refinement of its site occupancy indicates only a very minor Sb substitution (only 0.02 a.p.f.u. Sb). The coordination is completed by two additional bonds at ~3.2 Å.

The M2 and M4 sites are mixed (As, Sb) sites, with refined site occupancy $As_{0.60}Sb_{0.40}$ and $As_{0.66}Sb_{0.34}$, respectively. M2 has a three-fold coordination, with additional longer bonds at 2.9 and 3.3 Å; a similar coordination is shown by M4, with three shorter bonds and two longer ones, at 3.1 and 3.3 Å. According to Berlepsch *et al.* (2002) and considering only the bonds with *Me*−S distance <2.70 Å, M2 and M4 of rathite are pure As sites, with average bond lengths of 2.31 and 2.27 Å, respectively, compared with 2.39 and 2.35 Å of carducciite. In the crystal structure of barikaite, the M2 and M4 sites are labelled *Me*2 and *Me*3, respectively, and are mixed split (As, Sb) sites; according to Makovicky and Topa (2013), the split sub-positions indicate $As_{0.55}Sb_{0.45}$ for the *Me*2 site and $As_{0.82}Sb_{0.18}$ for *Me*3.

M3 is a pure Sb site, as indicated by the refinement of the As *vs.* Sb site-scattering value. Its average bond distance is 2.61 Å; M3 has two short bonds (2.44 and 2.46 Å) and two longer additional bonds (2.75 and 2.80 Å). This bond distribution is similar to that found by Berlepsch *et al.* (2002) for the split M3b position of rathite, which is occupied by arsenic; these authors reported two short bonds at 2.24 and 2.28 Å and two long bonds, at 2.69 and 2.73 Å. Whereas in rathite M3 is split into two sub-positions (M3a and M3b, occupied by $Sb_{0.265}$ and $As_{0.735}$, respectively), in carducciite there are no hints of such a splitting. In the crystal structure of barikaite, the M3 site is labeled as *Me*4 (Makovicky and Topa, 2013), and shows the same identical features observed in carducciite, that is a pure Sb occupancy and the same bond pattern, with an average bond distance of 2.61 Å.

The two split sites, M5 and M6, are occupied by Ag/Sb and Pb/As, respectively. The splitting of the M5 site was proposed by Marumo and Nowacki (1965), with Ag at the M5a sub-site (site occupancy factor (s.o.f.) 0.57) and As at M5b (s.o.f. 0.402). This was confirmed by Berlepsch *et al.* (2002), with Ag(M5a)/As(M5b) = 0.474/0.526; in barikaite, the Ag/As ratio is 0.53/0.47 (Makovicky and Topa, 2013). In carducciite, M5a hosts Ag (s.o.f. 0.526), with a distorted octahedral coordination and average bond length of 2.80 Å, in agreement with 2.77 Å observed by Berlepsch *et al.* (2002) for rathite and by Makovicky and Topa (2013) for barikaite. On the contrary, whereas the three-fold coordinated M5b positions of rathite and barikaite studied by these authors show a mean bond distance of 2.38 and 2.39 Å, respectively, the average bond distance of M5b observed in carducciite is significantly longer, i.e. 2.49 Å, ranging from 2.45 to 2.57 Å. The average bond distance and refined electron density at the M5b sub-position agree with an occupancy by Sb (s.o.f. 0.474). The M6 site is split into two sub-positions, namely M6a and M6b, hosting Pb (s.o.f. 0.92) and minor As (s.o.f. 0.08), respectively. M6a is a 'lying' monocapped trigonal prism, with average bond length of 3.04 Å. As also pointed out by Berlepsch *et al.* (2002), the coordination of M6b is not characteristic of arsenic, having four bonds ranging between 2.53 and 2.82 Å, and two longer bonds up to 3.53 Å. It is likely that, owing to the very low occupancy of the site, the exact positions of the associated S ligands cannot be resolved. Makovicky and Topa (2013) observed, for barikaite, the splitting of the M6 site into three sub-positions, namely Ag6, Pb6 and Sb6, with s.o.f. 0.28, 0.43 and 0.29, respectively.

Polymerization of $Me^{3+}S_3$ triangular pyramidal polyhedra

Marumo and Nowacki (1965) pointed out that in rathite "AsS_3 pyramids form chains with finite lengths", i.e. As_mS_n polymers. Re-examination of the structure indicates two possible combinations of two polymers: (1) As_3S_7 + As_6S_{13}, or (2) As_5S_{11} + As_4S_9. Refinement of the structure by Berlepsch *et al.* (2002) shows the validity of combination 2 (we do not take the mixed (Pb,As) M6 position into account). Such a polymeric organization was later recognized in various lead sulfosalts: andorite VI (Sawada *et al.*, 1987), sartorite (Berlepsch *et al.*, 2003), boscardinite (Orlandi *et al.*, 2012) and the pair sterryite/parasterryite (Moëlo *et al.*, 2012).

In carducciite, if only the shortest (= strongest) Me^{3+}–S bonds are considered (<2.70 Å – see Moëlo *et al.*, 2012), 'reduced' $(Sb/As)S_3$ triangular pyramidal polyhedra appear. The only exception is represented by the M3 site, which has only two bonds shorter than 2.70 Å; however, the third and fourth bonds (M3–S9 and M3–S8) are only a little longer, being ~2.75 and 2.80 Å, respectively. The projection perpendicular to **a** of one oblique ribbon of the dufrénoysite type (Fig. 4*a*) reveals the oblique stacking (~45° relative to the elongation) of finite 1D units elongated along $[100]_{PbS}$, with the ideal formula of carducciite, more exactly $AgPb_6Sb_3(As,Sb)_4As_2S_{20}$ (taking M6 = pure Pb, M1 = pure As and M5a = M5b = 0.50). Without Ag and Pb, $(Sb/As)S_3$ polyhedra constitute a single $Sb_3(As,Sb)_4As_2S_{20}$ polymer (Fig. 4*b*, No 1).

Nevertheless, in this polymer the M3 position appears to be a mean position, due to the long M3–S9 and M3–S8 bonds. Thus, when one of the two M3 positions is bound to S9, the second one must be bound to S8. Two choices are possible (Fig. 4*b*, No 2 and 3), but choice No 2 seems more probable. Indeed, there is a dissymmetry in the two M5b–M3 distances, a short one (3.60 Å) and a long one (3.89 Å). In choice No 3, the shift of M3 towards S9 will shorten the M5b–M3 distance below 3.60 Å, and thus increase the repulsion between these two Sb atoms. This is not the case in choice No 2, which appears more favourable from the energetic point of view. Considering this choice, the ordered structure would correspond to the combination of two polymers, $(As,Sb)_2AsS_7$ and $Sb_3(As,Sb)_2AsS_{13}$.

Crystal chemistry of the rathite sub-group of dufrénoysite homeotypes

Carducciite: a homeotypic derivative of dufrénoysite

The main characteristic of the crystal structure of carducciite is its derivation from the dufrénoysite pole by the complete coupled substitution $2Pb^{2+} = Ag^+ + Sb^{3+}$ at the M5 position. This substitution is a case of valency-imposed double site occupancy (Hatert and Burke, 2008). Such a coupled substitution leads to a space group ($P2_1/c$) distinct from that of dufrénoysite ($P2_1$): carducciite is a homeotype of dufrénoysite.

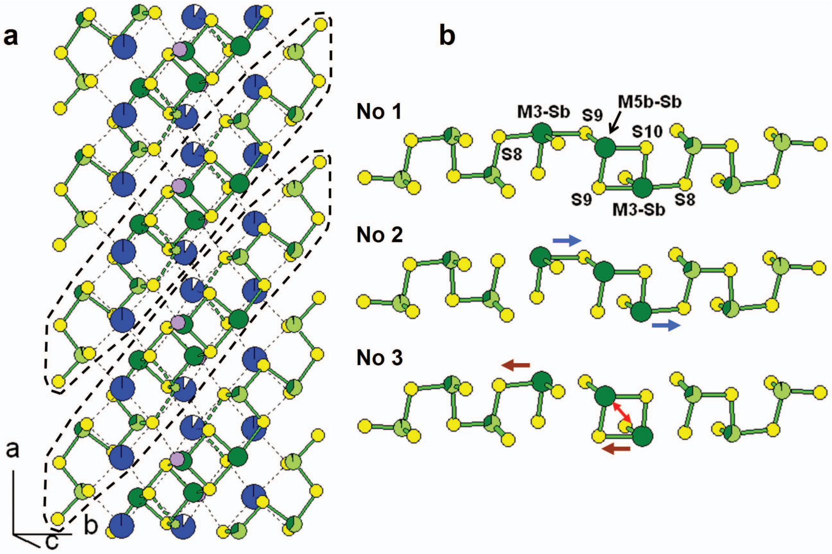

FIG. 4. Polymeric organization of the (Sb,As) atoms with S atoms (short bonds, green) in the dufrénoysite-type constitutive layer of carducciite. (*a*) Oblique stacking of 1D units (black shaded lines); (*b*) ideal $Sb_3(As,Sb)_4As_2S_{20}$ polymer. No 1: with M3 mean position; No 2: first sub-choice for the two effective M3 positions; No 3: second sub-choice. Horizontal blue or brown arrows indicate the shifts of M3 towards S8 or S9, and red double arrow the shortening of the M3−M5b distance. As/M6b with low s.o.f. [0.08 − small green circle in (*a*), with dashed As−S bond], has been omitted in (*b*).

The rathite sub-group of dufrénoysite homeotypes

Carducciite is closely related to rathite. It constitutes a specific mineral species, and not simply an Sb-rich variety of rathite, because of the specific crystal-chemical role played by Sb^{3+}, instead of As^{3+} in rathite, at the M5 position. Barikaite is also very close to rathite; its $P2_1/n$ setting, which is also given for rathite (Topa *et al.*, 2013), can be transformed conveniently into the conventional $P2_1/c$ setting through the transformation matrix R = (1 0 0, 0 $\bar{1}$ 0, $\bar{1}$ 0 $\bar{1}$), as suggested by Berlepsch *et al.* (2002). These relationships allow one to define the rathite sub-group of $P2_1/c$ homeotypes derived from the N = 4 dufrénoysite homologue. The unit-cell parameters of rathite, carducciite and barikaite in this $P2_1/c$ setting are reported in Table 8.

Crystal-chemical substitutions in the rathite sub-group

The available chemical data of rathite and barikaite are reported in Table 9. Another chemical analysis of rathite was reported by Nowacki and Bahezre (1963) but did not actually represent rathite, owing to the absence of Ag, contrasting with the structure solution of Marumo and Nowacki (1965) that indicated the occurrence of this element as an essential component. Consequently, this chemical data will not be accounted for.

Figure 5 shows the Pb content *vs.* (Sb + As) (Fig. 5*a*) and Ag (Fig. 5*b*) contents; Pb and (Sb + As) contents have been corrected by subtracting Tl. The tie-line in this figure represents the substitution $Me^{+} + Me^{3+} = 2\ Me^{2+}$ between dufrénoysite, $Pb_8As_8S_{20}$, and the hypothetical ideal endmember composition $Ag_2Pb_4(As,Sb)_{10}S_{20}$. In the framework of the N = 4 homologues of the sartorite series, with general formula $(Ag,Tl)_xPb_{8-2x}(As,Sb)_{8+x}S_{20}$, rathite and carducciite correspond to phases having $x = 1$, with ideal composition $AgPb_6(As,Sb)_9S_{20}$. Consequently, following Berlepsch *et al.* (2002), the chemical formulae of rathite and carducciite could conveniently be written as $(AgAs)Pb_6(As,Sb)_8S_{20}$ and $(AgSb)Pb_6(As,Sb)_8S_{20}$, respectively. Barikaite is close to the chemical pole having $x = 1.5$, $Ag_{1.5}Pb_5(As,Sb)_{9.5}S_{20}$; its crystal

TABLE 9. Electron microprobe chemical data of rathite and barikaite. Chemical analyses (in wt.%) were recalculated on the basis of ΣMe = 16 a.p.f.u. Ev values, $Pb_{corr.}$ and $(Sb + As)_{corr.}$ are calculated as in Table 2.

Element	1	1	1	1	2	2	2	3	4	4	4	4
Ag	4.18	4.04	3.86	4.13	3.50	3.90	3.85	3.46	5.51	5.87	4.55	4.93
Tl	3.49	5.10	4.41	5.36	2.10	1.35	0.90	1.07	0.13	0.13	0.07	0.22
Pb	39.49	36.62	38.51	36.61	43.9	44.8	45.4	45.48	36.18	35.50	39.21	38.19
As	25.68	26.85	26.59	27.31	26.3	25.9	25.3	25.74	15.52	15.77	15.38	15.18
Sb	2.95	2.42	2.05	1.94	0.15	0.35	0.75	n.d.	18.36	18.37	16.68	17.49
Fe	0.08											
S	24.50	24.77	24.31	24.48	23.7	24.4	23.7	24.54	23.92	23.98	23.65	23.66
Sum	100.37	99.80	99.74	99.82	99.17	100.6	100.00	100.29	99.62	99.63	99.55	99.68
ΣMe = 16 a.p.f.u.												
Ag	1.008	0.971	0.931	0.985	0.855	0.952	0.947	0.855	1.399	1.481	1.176	1.267
Tl	0.444	0.647	0.561	0.675	0.271	0.174	0.117	0.140	0.017	0.017	0.010	0.030
Pb	4.960	4.580	4.836	4.548	5.586	5.694	5.813	5.850	4.782	4.664	5.275	5.108
As	8.920	9.287	9.234	9.382	9.255	9.104	8.959	9.156	5.673	5.730	5.722	5.615
Sb	0.630	0.515	0.438	0.410	0.032	0.076	0.163		4.129	4.107	3.818	3.981
Fe	0.037											
S	19.883	20.019	19.725	19.649	19.487	20.039	19.610	20.395	20.428	20.358	20.557	20.448
Ev	0.8	0.4	1.8	2.1	3.0	−0.1	2.1	−1.6	−1.2	−0.9	−1.9	−1.5
$Pb_{corr.}$	5.848	5.874	5.958	5.898	6.128	6.042	6.047	6.130	4.816	4.698	5.295	5.168
$(Sb + As)_{corr.}$	9.106	9.155	9.111	9.117	9.016	9.006	9.007	9.016	9.785	9.820	9.530	9.566
$Sb/(Sb + As)_{at.}$	0.066	0.053	0.045	0.042	0.003	0.008	0.018	0.000	0.421	0.418	0.400	0.415

(1) Berlepsch *et al*. (2002); (2) Laroussi *et al*. (1989); (3) Graeser, unpublished data, in Pring (2001); (4) Topa *et al*. (2013).

chemical formula may be written $(Ag_{0.5}Sb_{0.5})(AgAs)Pb_5(As,Sb)_8S_{20}$.

In this multi-component series, starting from the pure Pb and As dufrénoysite pole, three kinds of substitution occur: (1) the homovalent substitution $As^{3+} = Sb^{3+}$; (2) the heterovalent substitution $2Pb^{2+} = Ag^+ + Me^{3+}$ ($Me^{3+} = As^{3+}$, Sb^{3+}); and (3) the heterovalent substitution $2Pb^{2+} = Tl^+ + Me^{3+}$.

The first substitution takes place, in particular, at the M3 site in rathite and carducciite, or its equivalent M4 site in barikaite, and, in minor amounts, at the M2 and M4 (= M3 in barikaite) sites (Table 10; see also Fig. 6). In particular, the M3 site has a refined site-occupancy $(As_{0.74}Sb_{0.26})$ in rathite from Lengenbach (Berlepsch *et al*., 2002), whereas it is a pure Sb site in carducciite and in M4 of barikaite. Indeed, carducciite and barikaite are richer in Sb than rathite, with an $Sb/(Sb+As)_{at.}$ ratio of 0.47 and 0.42 for carducciite and barikaite, respectively, to be compared with values ranging between 0 and 0.07 for rathite (Table 9).

The second substitution involves addition of Ag, which is required for the chemical stability of rathite, barikaite and carducciite with respect to dufrénoysite. The peculiar crystal-chemical role of silver in rathite (M5 site) was revealed by the crystal-structure study of Marumo and Nowacki (1965), refined by Berlepsch *et al*. (2002). It was enhanced by the electron microprobe analysis data of Laroussi *et al*. (1989). At the M5 site, the trivalent Me^{3+} cation could be As in rathite and barikaite, and Sb in carducciite (Table 10). Moreover, barikaite shows an Ag excess hosted at the M6 site, together with Sb.

Finally, rathite from Lengenbach has a variable but significant Tl content, ranging between 0.12 and 0.68 a.p.f.u. Carducciite and barikaite are quite Tl-free, showing only 0.13 and 0.15 wt.% Tl (detection limit, for carducciite analysis, 0.07 wt.%), corresponding to ~0.02 a.p.f.u. in both species. Thallium shows a clear negative correlation with lead and carducciite is actually richer in lead than rathite (5.91 a.p.f.u., whereas the values for rathite from Lengenbach range

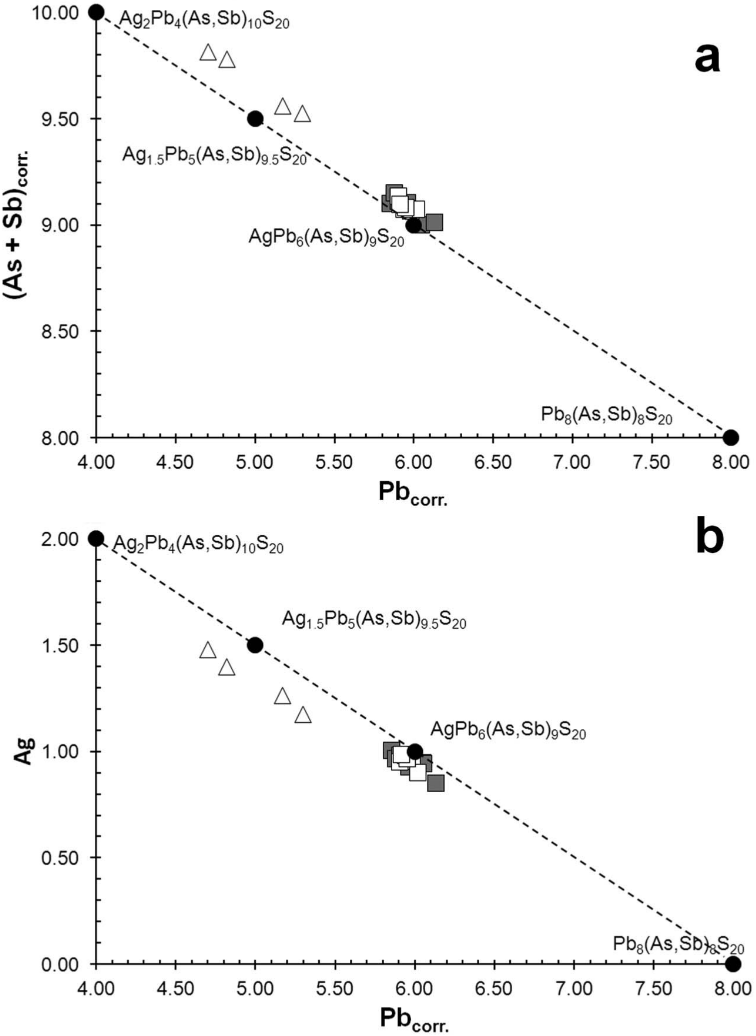

FIG. 5. Pb content (in a.p.f.u.) *vs*. (Sb + As) content (*a*) and Ag content (*b*) in the chemical formulae of members of the rathite sub-group. Triangles = barikaite. Squares: white = carducciite; grey = rathite. Circles = ideal compositions for x = 0, 1, 1.5 and 2.

between 4.55 and 5.85 a.p.f.u.). Thallium should be hosted at the Pb1 and/or Pb2 sites, in agreement with its typical nine-fold coordination in other sulfosalts, e.g. boscardinite (Orlandi *et al*., 2012). If thallium occurs, then the Pb site M6 would be partly occupied by Me^{3+} cations, in accordance with the 2 $Pb^{2+} = Tl^{+} + Me^{3+}$ substitution. This is in agreement with structural data that indicate, for thallium-bearing rathite from Lengenbach, a site occupancy of $Pb_{0.74}As_{0.26}$ (although Tl has not been localized at Pb1 or Pb2 sites). On this basis, refining Pb *vs.* As at the M6 split site of carducciite, a site occupancy $Pb_{0.91}As_{0.09}$ is proposed, corresponding to 0.18 a.p.f.u., in agreement with a minor importance of the $2Pb^{2+} = Tl^{+} + Me^{3+}$ substitution. Nevertheless, it is not clear if Me^{3+} is preferentially arsenic or antimony. In fact, the bond distances for the M6b split site in rathite and carducciite are unusual for arsenic in trigonal pyramid coordination. According to Berlepsch *et al*. (2002) it could be due to the low site occupancy of this position, and the consequent impossibility of resolving the S disorder associated with the Pb−As substitution. However, the

TABLE 10. Cation site occupancy in rathite, barikaite and carducciite. Corresponding pairs of cations in dufrénoysite are given for comparison. *SP*: different cations in split positions. The order of M sites corresponds to their positions from the border to the centre of their constitutive polymeric units.

Dufrénoysite	Rathite		Barikaite		Carducciite	
(Pb1, Pb4) and	Pb1		Pb1		Pb1	
(Pb2, Pb3)	Pb2		Pb2		Pb2	
As2 and As3	M1	As 1.00	M1	As 1.00	M1	As 0.98 Sb 0.02
As1 and As4	M2	As 1.00	M2 *SP*	As 0.549 Sb 0.451	M2	As 0.60 Sb 0.40
As8 and As5	M4	As 1.00	M3 *SP*	As 0.821 Sb 0.179	M4	As 0.66 Sb 0.34
Pb7 and As6	M3 *SP*	As 0.735 Sb 0.265	M4	Sb 1.00	M3	Sb 1.00
Pb8 and Pb6	M6 *SP*	Pb 0.739 As 0.261	M6 *SP*	Pb 0.434 Ag 0.279 Sb 0.287	M6 *SP*	Pb 0.92 As 0.08
As7 and Pb5	M5 *SP*	As 0.526 Ag 0.474	M5 *SP*	Ag 0.529 As 0.471	M5 *SP*	Ag 0.526 Sb 0.474

possibility of a Pb–Sb substitution could not be excluded, as observed in other phases of the sartorite homologous series and particularly in boscardinite (Orlandi *et al*., 2012) and barikaite (Makovicky and Topa, 2013). Moreover, chemical data for rathite from Lengenbach indicates the existence of a Tl-bearing variety of rathite, containing ~0.5 Tl p.f.u., and a Tl-poor variety, hosting <0.30 a.p.f.u. of thallium (Table 9). It is noteworthy that the former shows ~1 a.p.f.u. of Sb, whereas in the latter Sb is scarce or absent. Actually, as exemplified by barikaite, the M6 site is quite flexible, able to host Pb^{2+}, As^{3+}, Sb^{3+}, as well as Ag^{+}.

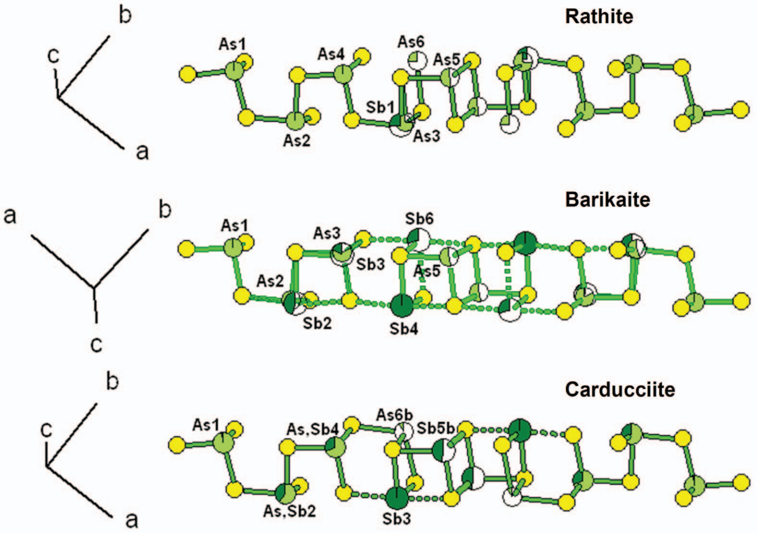

FIG. 6. Comparison of polymeric units of rathite, barikaite and carduccite. Only Me^{3+} cations have been represented. Dark green circle/area: Sb; light green circle/area: As. Straight line: strong bond; tie-line: medium bond.

TABLE 11. Chemical variations in Ag-Pb sulfosalts from the Pollone mine.

	$As/(Sb+As)_{at.}$	$Pb/(Sb+As±Bi)_{at.}$	$Pb/(Ag±Cu±Tl±Hg)_{at.}$	Ref.
Carducciite	0.531	0.649	6.03	[1]
Meerschautite	0.153	0.951	7.095	[2]
Owyheeite	0.099	0.924	4.361	[3]*
Parasterryite	0.391	0.859	5.329	[4]
Sb-poor sterryite	0.392	0.764	4.33	[4]
Sb-rich sterryite	0.260	0.784	4.71	[4]

* Average of two chemical points. [1] this work; [2] Biagioni *et al*. (in prep.); [3] Carmignani *et al*. (1976); [4] Moëlo *et al*. (2011).

Distinction between carducciite, barikaite and rathite

Barikaite, carducciite and rathite are homeotypic derivatives of dufrénoysite, having a different space group. This corresponds to the first criterion of distinction between homeotypy and isotypy, as defined by Lima-de-Faria *et al*. (1990). Although these three species have the same space group, with close unit cells, they are homeotypes according to the second criterion, i.e. when in one structure one cation position is replaced by a split position in the other (distinct topologies). This is realized when, for instance, a pure As site is replaced by a split (As, Sb) site (compare M2 sites of rathite and barikaite in Table 10).

Generally, close homeotypes correspond to distinct mineral species, as exemplified by the numerous members of the aikinite-bismuthinite homeotypic series (Moëlo *et al*., 2008). But it is not always the case, particularly in the field of sulfosalts, when there are mixed $(Sb, As)^{3+}$ sites. In the majority of such compounds, Sb^{3+} and As^{3+} have a dissymmetric coordination, with three short bonds, due to the high stereochemical activity of their lone electron pair. In mixed (Sb, As) sites, as As−S bonds are shorter than Sb−S bonds (ideally 2.26 and 2.45 Å, respectively), Sb and As will have necessarily distinct sub-positions in the S polyhedron, although with the same topology. If, for instance, in a pure As sulfosalt minor Sb substitutes for As in at least one As site (without any structural change), this Sb-enriched derivative will be a homeotypic derivative of the pure As pole, but always corresponding to the same mineral species. As an example, if there exists (very probably) an Sb-free rathite, it will be a homeotype of Sb-containing rathite, due to the split M3 position (Table 10).

Another homeotypic differentiation is an artifact due to the quality of structure resolution. For instance, in carducciite all mixed (As, Sb) sites are unsplit positions, while they are split in barikaite. On the basis of this sole characteristic, barikaite and carducciite are homeotypes, but it is due to the poor quality of the single crystal of carducciite, which did not allow the Sb and As sub-positions at the M2 and M4 sites to be differentiated.

In some cases, Sb presents only two short bonds, together with medium ones: Sb3 in carducciite, Sb2 and Sb4 in barikaite (Fig. 6). Such sites may correspond to the mean of two sub-positions, determining two distinct polymeric units (see above for carducciite). In barikaite, Sb2 is associated with a well-defined As2 position; one of the Sb2 sub-positions is topologically identical to As2, but not the other.

This general approach is also valuable in sulfosalt systematics for other mixed sites with very distinct cations (size, type of coordination): Pb *vs.* (Ag + Sb), Bi *vs.* Sb etc.

As a consequence, we consider that homeotypy cannot be a criterion for the distinction between rathite, barikaite and carducciite as mineral species. Only chemical variations in the filling of *Me* sites have to be taken into account, here on the basis of the criterion of the 50% limit of substitution. According to Table 10: (1) there are no significant changes in M1, M2 and M4 (= M3 in barikaite). In particular, Sb s.o.f. in barikaite and carducciite are always below the 50% limit. (2) As predominates at M3 of rathite, while M4 of barikaite and M3 of carducciite are pure Sb sites; (3) Pb predominates at M6 of rathite and carducciite, while (Ag + Sb) surpasses the 50% limit in barikaite, according to the $2\ Pb^{2+} = Ag^{+} +$

Sb^{3+}substitution; (4) in the mixed (Ag^{+}, Me^{3+}) M5 site, As predominates in rathite and barikaite, against Sb in carducciite.

In the CNMNC-IMA proposal, carducciite has been defined as a distinct species relative to rathite on the sole basis of the filling of the M5 site, i.e. (Ag + Sb), against (Ag + As) in rathite. The pure Me^{3+} sites (M1 to M4) have been considered as a whole, with a mean Sb ratio below the 50% limit (47%). Thus, the limit between carducciite and rathite would correspond to the 50% limit within the M5 position, i.e. ($Ag_{0.50}Sb_{0.25}As_{0.25}$).

In their definition of barikaite, Topa *et al.* (2013) point out the ordered distribution of As and Sb among pure Me^{3+} sites, that "represents a feature which separates it from rathite". In particular, they apply the criterion of the 50% limit to the pure Sb M4 site alone, corresponding to the split (As, Sb) M3 site of rathite, to distinguish these two species. Similarly, in the modular description of the barikaite structure, Makovicky and Topa (2013) take into account the shortest (As, Sb)−S bonds to distinguish finite crank-shaft chains (i.e. $(As, Sb)_mS_n$ polymers as indicated above), which have different sizes from those observed in rathite. It is this difference, together with As/Sb ordering, which controls the homeotypic derivation of barikaite from rathite, and thus the distinction between these two species.

As stated above, a small shift of the Sb/As ratio in such complex structures may induce homeotypic changes, and different polymeric units, related to Sb/As ordering, in an unchanged mineral species. For instance, M2 sites of barikaite and carducciite have an Sb content just below the 50% limit. With a small increase of the mean Sb/As ratio, Sb s.o.f. may surpass such a limit: according to Topa *et al.* (2013), such a change would induce a new mineral species. We think that such a detailed crystal-chemical analysis is not strictly pertinent in the field of mineral systematics.

In barikaite, the $Sb/(As+Sb)_{at.}$ mean ratio of pure Me^{3+} sites is 0.41, clearly below the 50% limit, and lower than in carducciite (47%). According to our approach, it would not justify its distinction from rathite. On the contrary, a specific feature of barikaite is the substitution of (Ag+Sb) to 2Pb at the M6 site, over the 50% limit (56%). This could be taken as the criterion for the definition of barikaite relative to rathite, as well as carducciite. On this basis, the structural formulae for the rathite sub-group would be ($\Sigma\ Me$ = 16 a.p.f.u.):

(1) rathite (low Ag, Sb low or absent): $^{M5}(AgAs)^{M6}Pb_2Pb_4(As,Sb)_8S_{20}$;

(2) barikaite (high Ag, high Sb): $^{M5}(AgAs)^{M6}(Ag_{0.5+x}Sb_{0.5+x}Pb_{1-2x})Pb_4(As,Sb)_8S_{20}$ ($0 < x < 0.5$);

(3) carducciite (low Ag, higher Sb): $^{M5}(AgSb)^{M6}Pb_2Pb_4(As,Sb)_8S_{20}$.

Relationship with sterryite and parasterryite

During the study of sterryite and parasterryite, Moëlo *et al.* (2011) noted that in the pseudoternary system $Pb_2S_2-(Sb,As)_2S_3-(Ag,Cu)_2S$, the sulfosalts closest chemically are the owyheeite solid-solution field and rathite. Owyheeite has been reported previously from the Pollone mine by Carmignani *et al.* (1976) on the basis of electron microprobe data. Carducciite occurs in the same assemblage as sterryite; it is noteworthy that Moëlo *et al.* (2011) emphasized that parasterryite can be considered a perfect mixture of owyheeite and Tl-free rathite. As discussed in this present paper, carducciite is the Sb-rich, Tl-free homeotype of rathite, and appears more appropriate as the As-rich component, together with owyheeite, of the sterryite 'mixture'.

The occurrence of such sulfosalts (Table 11) indicates the great potential of the Pollone mine for the study of the paragenetic relationships between Ag sulfosalts. At Pollone, these phases are the result of reactions and recrystallizations during Alpine metamorphism. Up to now, carducciite has only been observed embedded in the granoblastic baryte, whereas sterryite and parasterryite also occur in late-stage cavities. However, a detailed study of the textural relationships between these phases is necessary to understand the evolution of the hydrothermal system at the Pollone mine.

Conclusion

The occurrence of carducciite at the Pollone mine brings useful new data to our knowledge of the sartorite homologous series and of the phase equilibria in the $PbS-Ag_2S-As_2S_3-Sb_2S_3$ system. The richness in Sb of carducciite with respect to rathite agrees with the usual crystal chemistry of Pb sulfosalts from Apuan Alps. Sb-rich analogues or varieties of As sulfosalts were described, for example, from the Monte Arsiccio mine, i.e. boscardinite, the Tl-Sb homeotype of baumhauerite, and e.g. protochabournéite (Orlandi *et al.*, 2012, 2013).

The crystal chemistry of the dufrénoysite homeotypic series points to several questions which must be clarified. The crystal structure of veenite, the Sb-rich derivative of dufrénoysite (Jambor, 1967) must be resolved, in order to examine the distribution of Sb among primitive As positions of dufrénoysite. In the rathite subgroup, there is a competition starting from rathite between the Sb enrichment, which favours the incorporation of Sb at the M5 position, and the Ag enrichment, which maintains As at the M5 position, but promotes Sb incorporation at the M6 position. The limit between these two very close trends, which determines the distinction between barikaite and carducciite, remains unknown. Another question is the limit between rathite and carducciite, i.e. what is the Sb/As ratio in the solid solution controlling the $(Ag_{0.50}Sb_{0.25}As_{0.25})$ limit on the M5 position?

Acknowledgements

Electron microprobe analyses were performed with the help of O. Rouer (CNRS engineer, Institut des Sciences de la Terre d'Orléans). The paper was handled by Allan Pring; the comments of Dan Topa and an anonymous referee helped to improve the paper.

References

Baumhauer, H. (1896) Ueber den Rathit, ein neues mineral aus dem Binnenthaler Dolomit. *Zeitschrift für Kristallographie*, **26**, 593–602.

Berlepsch, P., Armbruster, T. and Topa, D. (2002) Structural and chemical variations in rathite, $Pb_8Pb_{4-x}(Tl_2As_2)_x(Ag_2As_2)As_{16}S_{40}$: modulations of a parent structure. *Zeitschrift für Kristallographie*, **217**, 581–590.

Berlepsch, P., Armbruster, T., Makovicky, E. and Topa, D. (2003) Another step toward understanding the true nature of sartorite: determination and refinement of a ninefold superstructure. *American Mineralogist*, **88**, 450–461.

Biagioni, C., Orlandi, P., Moëlo, Y., Pardini, S. and Passarino, G. (2012) Sterryite e parasterryite. I solfosali aciculari di piombo e argento della miniera del Pollone (Pietrasanta, Lucca). *Rivista Mineralogica Italiana*, **2/2012**, 76–91.

Biagioni, C., Moëlo, Y., Orlandi, P., Stanley, C.J. and Evain, M. (2013*a*) Meerschautite, IMA 2013-061. CNMNC Newsletter No. 17, October 2013, page 3004. *Mineralogical Magazine*, **77**, 2997–3005.

Biagioni, C., Orlandi, P. and Moëlo, Y. (2013*b*) Carducciite, IMA 2013-006. CNMNC Newsletter No. 16, August 2013, page 2702. *Mineralogical Magazine*, **77**, 2695–3709.

Brese, N.E. and O'Keeffe, M. (1991) Bond-valence parameters for solids. *Acta Crystallographica*, **B47**, 192–197.

Bruker AXS Inc. (2004) APEX 2. Bruker Advanced X-ray Solutions, Madison, Wisconsin, USA.

Cannon, R., Hensel, H. and Raber, T. (2008) Der Reckibach-Dolomit im Binntal, Schweiz: Mineralbestand und Neufunde. *Lapis*, **33**, 20–28.

Carmignani, L., Dessau, G. and Duchi, G. (1976) I giacimenti a barite, pirite ed ossidi di ferro delle Alpi Apuane. Studio minerogenetico e strutturale. *Bollettino della Società Geologica Italiana*, **95**, 1009–1061.

Costagliola, P., Benvenuti, M., Lattanzi, P. and Tanelli, G. (1998) Metamorphogenic barite-pyrite (Pb-Zn-Ag) veins at Pollone, Apuane Alps, Tuscany: vein geometry, geothermobarometry, fluid inclusions and geochemistry. *Mineralogy and Petrology*, **62**, 29–60.

Hatert, F. and Burke, E.A.J. (2008) The IMA-CNMNC dominant-constituent rule revisited and extended. *The Canadian Mineralogist*, **46**, 717–728.

Jambor, J.L. (1967) New lead sulfantimonides from Madoc, Ontario – Part 1. *The Canadian Mineralogist*, **9**, 7–24.

Kraus, W. and Nolze, G. (1996) POWDER CELL – a program for the representation and manipulation of crystal structures and calculation of the resulting X-ray powder patterns. *Journal of Applied Crystallography*, **29**, 301–303.

Laroussi, A., Moëlo, Y., Ohnenstetter, D. and Ginderow, D. (1989) Argent et thallium dans les sulfosels de la série de la sartorite (Gisement de Lengenbach, vallée de Binn, Suisse). *Comptes Rendus de l'Académie des Sciences, Paris*, **308 (Série II)**, 927–933.

Lima-de-Faria, J., Hellner, E., Liebau, F., Makovicky, E. and Parthé, E. (1990) Nomenclature of inorganic structure types. Report of the IUCr Commission on Crystallographic Nomenclature Subcommittee on the Nomenclature of Inorganic Structure Types. *Acta Crystallographica*, **A46**, 1–11.

Makovicky, E. (1985) The building principles and classification of sulphosalts based on the SnS archetype. *Fortschritte der Mineralogie*, **63**, 45–89.

Makovicky, E. and Topa, D. (2013) The crystal structure of barikaite. *Mineralogical Magazine*, **77**, 3093–3104.

Marumo, F. and Nowacki, W. (1965) The crystal structure of rathite-I. *Zeitschrift für Kristallographie*, **122**, 433–456.

Marumo, F. and Nowacki, W. (1967) The crystal structure of dufrenoysite, $Pb_{16}As_{16}S_{40}$. *Zeitschrift für Kristallographie*, **124**, 409–419.

Moëlo, Y., Makovicky, E., Mozgova, N.N., Jambor, J.L., Cook, N., Pring., A., Paar, W.H., Nickel, E.H., Graeser, S., Karup-Møller, S., Balić-Žunić, T., Mumme, W.G., Vurro, F., Topa, D., Bindi, L., Bente, K. and Shimizu, M. (2008) Sulfosalt systematics: a review. Report of the sulfosalt sub-committee of the IMA Commission on Ore Mineralogy. *European Journal of Mineralogy*, **20**, 7–46.

Moëlo, Y., Orlandi, P., Guillot-Deudon, C., Biagioni, C., Paar, W. and Evain, M. (2011) Lead-antimony sulfosalts from Tuscany (Italy). XI. The new mineral species parasterryite, $Ag_4Pb_{20}(Sb_{14.5}As_{9.5})_{\Sigma 24}S_{58}$, and associated sterryite, $Cu(Ag,Cu)_3Pb_{19}(Sb,As)_{\Sigma 22}(As{-}As)S_{56}$, from the Pollone mine, Tuscany, Italy. *The Canadian Mineralogist*, **49**, 623–638.

Moëlo, Y., Guillot-Deudon, C., Evain, M., Orlandi, P. and Biagioni, C. (2012) Comparative modular analysis of two complex sulfosalt structures: sterryite, $Cu(Ag,Cu)_3Pb_{19}(Sb,As)_{22}(As\text{-}As)S_{56}$, and parasterryite, $Ag_4Pb_{20}(Sb,As)_{24}S_{58}$. *Acta Crystallographica*, **B68**, 480–492.

Nowacki, W. and Bahezre, C. (1963) Die bestimmung der chemischen Zusammensetzung einiger Sulfosalze aus dem Lengenbach (Binnatal, Kt. Wallis) mit Hilfe der elektronischen Mikrosonde. *Schweizerische Mineralogische und Petrographische Mitteilungen*, **43**, 407–411.

Orlandi, P., Biagioni, C., Bonaccorsi, E., Moëlo, Y. and Paar, W.H. (2012) Lead-antimony sulfosalts from Tuscany (Italy). XII. Boscardinite, $TlPb_4(Sb_7As_2)_{\Sigma 9}S_{18}$, a new mineral species from the Monte Arsiccio mine: occurrence and crystal structure. *The Canadian Mineralogist*, **50**, 235–251.

Orlandi, P., Biagioni, C., Moëlo, Y., Bonaccorsi, E. and Paar, W.H. (2013) Lead-antimony sulfosalts from Tuscany (Italy). XIII. Protochabournéite, $\sim Tl_2Pb(Sb_{9\text{-}8}As_{1\text{-}2})_{\Sigma 10}S_{17}$, from the Monte Arsiccio mine: occurrence, crystal structure and relationship with chabournéite. *The Canadian Mineralogist*, **51**, 475–494.

Pandeli, E., Bagnoli, P. and Negri, M. (2004) The Fornovolasco schists of the Apuan Alps (Northern Tuscany, Italy): a new hypothesis for their stratigraphic setting. *Bollettino della Società Geologica Italiana*, **123**, 53–66.

Pring, A. (2001) The crystal chemistry of the sartorite group minerals from Lengenbach, Binntal, Switzerland – a HRTEM study. *Schweizerische Mineralogische und Petrographische Mitteilungen*, **81**, 69–87.

Sawada, H., Kawada, I., Hellner, E. and Tokonami, M. (1987) The crystal structure of senandorite (andorite VI): $PbAgSb_3S_6$. *Zeitschrift für Kristallographie*, **180**, 141–150.

Sheldrick, G.M. (2008) A short history of SHELX. *Acta Crystallographica*, **A64**, 112–122.

Topa, D., Makovicky, E., Tajedin, H., Putz, H. and Zagler, G. (2013) Barikaite, $Pb_{10}Ag_3(Sb_8As_{11})_{\Sigma 19}S_{40}$, a new member of the sartorite homologous series. *Mineralogical Magazine*, **77**, 3039–3046.

Wilson, A.J.C. (editor) (1992) *International Tables for Crystallography Volume C: Mathematical, Physical and Chemical Tables*. Kluwer Academic Publishers, Dordrecht, The Netherlands.